Microsc. Microanal. 12, 442–455, 2006
DOI: 10.1017/S1431927606060600

Microscopy AND Microanalysis

Advancing the Hexapole C_s-Corrector for the Scanning Transmission Electron Microscope

Heiko Müller,* Stephan Uhlemann, Peter Hartel, and Maximilian Haider

Corrected Electron Optical Systems GmbH, Englerstr. 28, D-69126 Heidelberg, Germany

Abstract: Aberration correctors using hexapole fields have proven useful to correct for the spherical aberration in electron microscopy. We investigate the limits of the present design for the hexapole corrector with respect to minimum probe size for the scanning transmission electron microscope and discuss several ways in which the design could be improved by rather small and incremental design changes for the next generation of advanced probe-forming systems equipped with a gun monochromator.

Key words: aberration, corrector, STEM, hexapole, monochromator, probe size, resolution

Introduction

Correctors compensating for the spherical aberration C_s of the objective lens are available for a large variety of transmission electron microscopes (TEM) from different manufacturers. C_s-corrected imaging is becoming more and more a well-accepted technique for materials science applications. Correctors exist for the probe-forming system of the scanning TEM (STEM) as well as for the imaging system of the conventional TEM (CTEM). Even double-corrected systems with two correctors integrated in one column have been installed (Hutchison et al., 2005) and are operating routinely.

Although for the CTEM so far only the hexapole corrector has proven useful (Haider et al., 1998), for the STEM two competitive designs exist, the quadrupole-octupole corrector (Krivanek et al., 1999) and the hexapole corrector.

For both correctors operating at a beam voltage of 300 kV it has been shown that the 78 pm dumbbell spacing in Si⟨112⟩ can be clearly resolved by annular dark-field (ADF) imaging (Nellist et al., 2004). Corresponding results for the hexapole corrector are shown in Figure 1. This image has been taken with a CEOS hexapole STEM corrector (CESCOR) integrated in a FEI Titan 80-300 microscope. Using the same system Erni et al. (2006) have resolved the 89-pm dumbbell spacing in diamond C⟨110⟩.

Theoretical investigations reported recently for the quadrupole-octupole design (Delby et al., 2005) as well as for the hexapole design (Müller et al., 2005) show that a further improvement with respect to STEM probe size, and also with respect to STEM resolution, should be possible if the energy width of the gun is sufficiently small. According to the information given by Delby et al. (2005) for the quadrupole-octupole corrector, a completely new design is required to enable such a further improvement. Compared to the previous design, the complexity of the new quadrupole-octupole corrector system increases considerably to avoid limiting fifth-order residual aberrations.

In general quadrupole-octupole systems introduce third-order axial aberrations of multiplicities zero, two, and four and fifth-order axial aberrations of multiplicity zero, two, four, and six. The third-order aberrations can be canceled by placing octupole fields at appropriate planes or can be avoided by a symmetric design of the system. For the fifth-order axial aberrations the situation is more involved. A direct compensation of fifth-order axial aberrations would require dodecapole fields. Alternatively, fifth-order aberrations can be avoided or at least kept small by a carefully chosen symmetric arrangement of the quadrupole and octupole elements, but this results in a more complicated system with a stack of nine or more multipole stages (Krivanek et al., 2003; Rose, 2004).

For the present design of the hexapole corrector with only two multipole stages, the first uncorrected residual intrinsic aberration is the fifth-order sixfold astigmatism, which can limit the attainable minimum probe size for large aperture angles. The fifth-order spherical aberration of a hexapole-corrected system can be tuned between positive and negative values. This makes the sixfold astigmatism the only limiting fifth-order axial aberration for the hexapole design.

In the following, we will show that both the sixfold astigmatism and the fifth-order spherical aberration can be strongly suppressed or even completely eliminated simultaneously by small, incremental changes of the optical design of the present STEM hexapole corrector. Furthermore, we will characterize the expected performance for a future

Received December 13, 2005; accepted July 27, 2006.
*Corresponding author. E-mail: mueller@ceos-gmbh.de

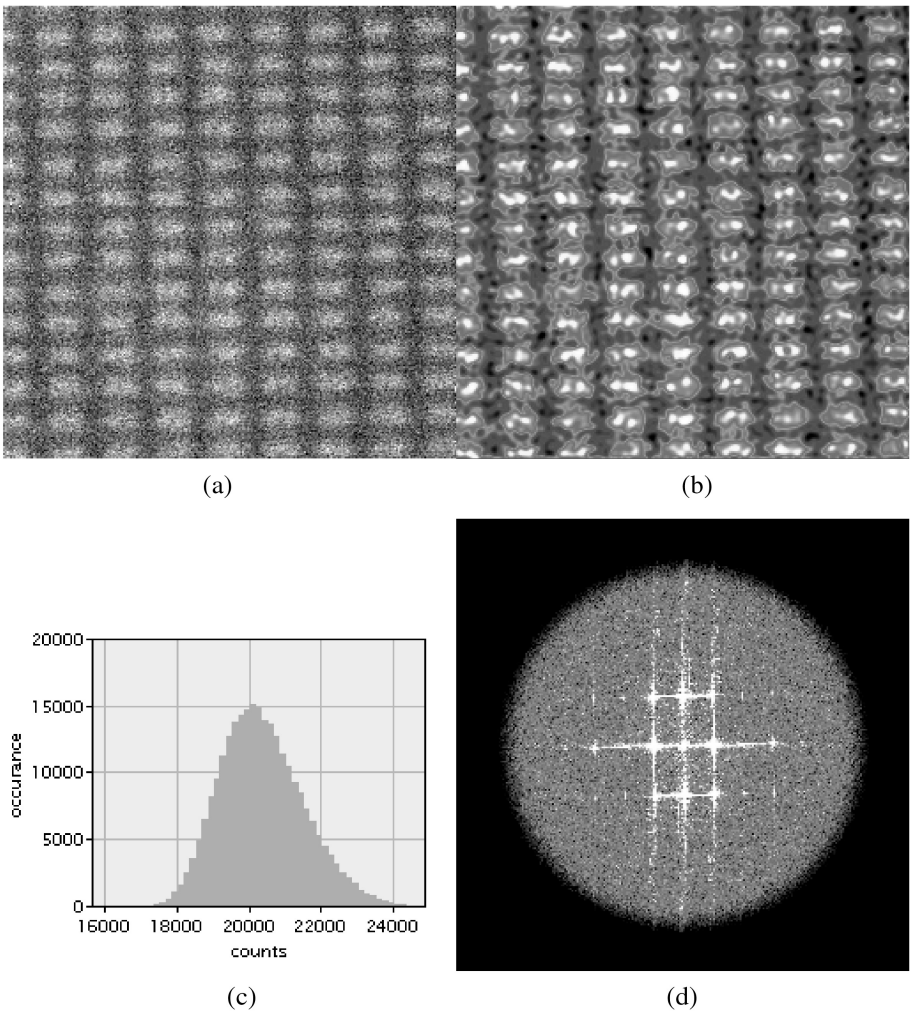

Figure 1. Raw data of a STEM ADF image of Si⟨112⟩ (**a**) recorded with a hexapole STEM corrector (CESCOR) in a FEI Titan 80-300 microscope operated at 300 kV. A region of 256 × 256 pixels of an image with 512 × 512 pixels is shown. The histogram (**c**) demonstrates that the signal of the dark-field detector was not clipped. In the low-pass filtered image (**b**), the dumbbell structure corresponding to the (444) spacing of 78 pm is clearly resolved. The modulus of the Fourier transform of the 512 × 512 image together with the low-pass filter can be seen in (**d**).

high-resolution STEM equipped with an advanced hexapole corrector and a field-emission gun with monochromator (MC-FEG).

Materials and Methods

Present Design of the Corrector

The optical design of the present hexapole corrector for the STEM is depicted schematically in Figure 2. The corrector is integrated in the probe-forming system of a TEM column between the last condenser lens and the objective lens. It consists of two principal hexapole elements (HP1, HP2), five transfer lenses (TL11/TL12, TL21/TL22, ADL), eight *x*/*y* alignment deflectors (DP11/DP12, DP21/DP22, DPH1/DPH2, BTlt, BSh), and two stigmators (QPol/HPol) for twofold and threefold astigmatism.

If available, the condenser-side minilens of the TEM is used as a replacement for the lower transfer lens TL11, and properly weighted DC offsets to the upper and lower scan coils emulate the deflector DP12.

The strong principal hexapole fields (HP1/HP2) are generated by two multipole elements, each with six ferromagnetic pole pins. The assembly of one of the hexapole elements with pole pins, pole pieces, coils, and yoke is shown in Figure 3. For the present electro-mechanical design, the central bore of the multipole element has a radius of $R_{HP} = 4$ mm, and the pole pieces have a length of $L_{HP} = 30$ mm measured along the optic axis. A nickel–iron alloy is used as material for the pole pins to allow for accurate and reproducible magnetic fields.

In Figure 2, the course of the axial fundamental ray u_α and of a selected field ray u_γ are depicted. The field ray u_γ is chosen such that it has a zero at the coma-free aperture plane situated close to the front focal plane (ffp) of the objective lens. The beam path and the fields inside the core corrector consisting of the pair of hexapoles HP1/HP2 with the transfer doublet TL21/TL22 in between are double-symmetric with respect to the midplanes of the hexapole fields and to the midplane between TL21 and TL22. The

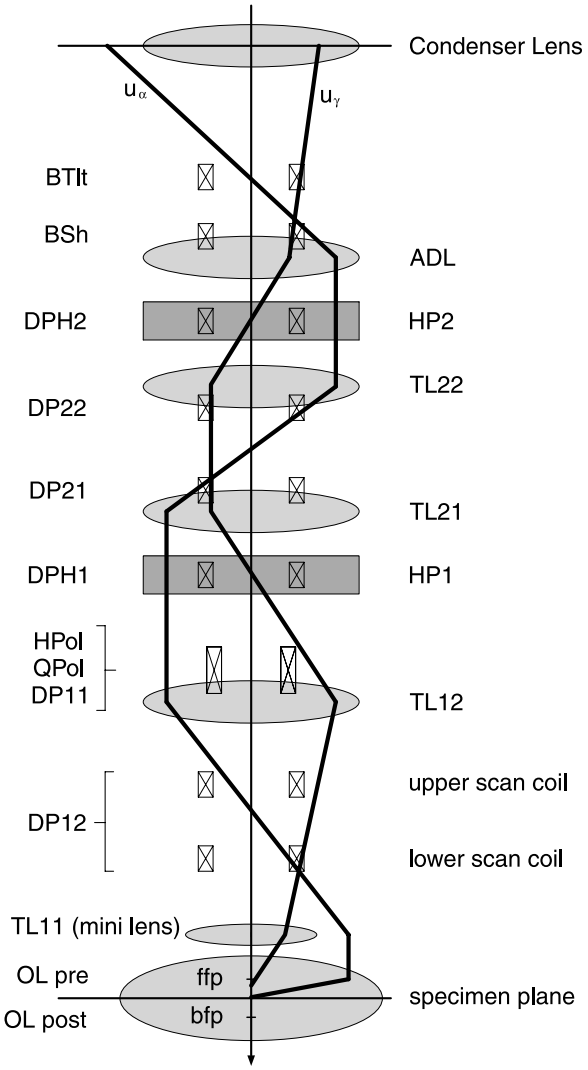

Figure 2. Schematic drawing of the optical design of a hexapole STEM corrector with transfer lenses (TL), adaptor lens (ADL), hexapole elements (HP), alignment deflectors (DP), beam tilt (BTlt) and beam shift (BSh) coils, and stigmators (QPol, HPol). In addition, the courses of the axial ray u_α and of a selected field ray u_γ are depicted.

transfer system TL11/TL12 between corrector and OL makes the coma-free aperture plane and the midplanes of both hexapole fields optically conjugated with respect to each other. The magnification M_{TL} between these planes can be used to adjust the correction strength of the corrector. An image of the source is located near DP12, at the symmetry plane of TL21/TL22, and above the adapter lens ADL. The excitation of the ADL and of the last condenser lens can be used as an aperture zoom to tune the STEM probe semi-angle without changing the physical condenser aperture.

STEM Probe Size

To assess the achievable minimum probe size in a STEM equipped with a C_s-corrector, the residual optical aberrations, the chromatic focus spread, and noise induced effects must be considered. The *residual intrinsic aberrations* are due to the optical design of the corrector. These aberrations are present also for the perfectly manufactured and aligned system and can be calculated reliably in advance. Unfortunately, such an idealized system does not exist in reality. Manufacturing tolerances, material inhomogeneities, and misalignment cause additional *parasitic aberrations*. For a well-aligned system, the relevant parasitic aberrations should be compensated. This compensation cannot be perfect and the amount of *residual parasitic aberrations* depends on the efficiency of the available procedures for semiautomatic alignment.

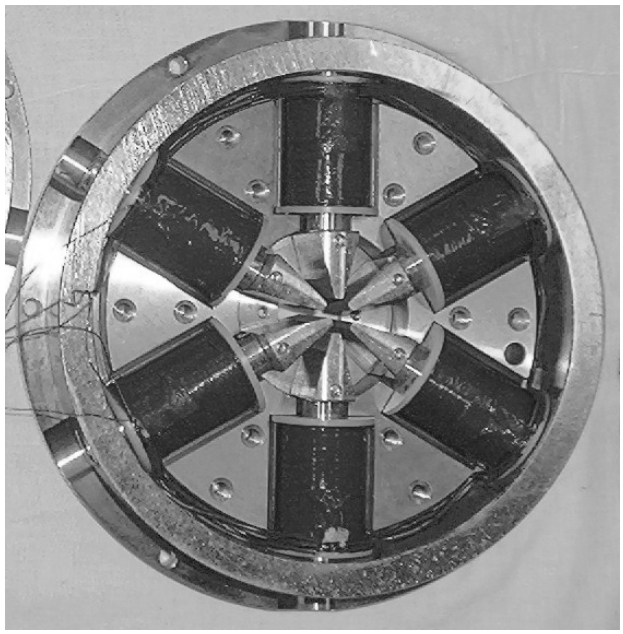

Figure 3. Single hexapole element of the present STEM hexapole corrector having six ferro-magnetic pole pins with pole pieces, coils, and yoke. The outer diameter of the yoke is 152 mm. The liner tube inside the hexapole bore is not shown in this picture.

The *chromatic focus spread* is proportional to the product of the relative root mean square energy width $\sigma(E)/E_0$ of the source and the total axial chromatic aberration C_c of the probe-forming system, including contributions of the gun lens, the condenser lenses, the corrector's transfer lenses, and the objective lens. Under high-resolution conditions, the contribution of the objective lens is strongly dominant. The total chromatic aberration is determined by the optical design, whereas the energy width can be reduced by a gun monochromator (MC). Due to the loss of beam current, the MC typically also reduces the brightness of the gun.

To account for the effects of noise, the induced focus spread and image spread must be considered. Unstable lens currents introduce *noise-induced focus spread*. Assuming Gaussian distributions for the energy spread $\sigma(E)$ of the electron source, for the high-voltage ripple $\sigma(U)$, and the

noise on the objective lens current $\sigma(I)$, the contributions to the total root mean square focus spread $\sigma(C_1)$ ($C_1 = -\Delta f$ denotes the eikonal coefficient of defocus) add up quadratically

$$\sigma^2(C_1) = \left(\left(\frac{\sigma(E)}{E} \right)^2 + \left(\frac{\sigma(U)}{U} \right)^2 + \left(\frac{\sigma(I)}{I} \frac{2 + \frac{E}{mc^2}}{1 + \frac{E}{mc^2}} \right)^2 \right) C_c^2, \qquad (1)$$

where m and c denote the mass of rest of the electron and the vacuum speed of light, respectively. It should be noted that for a strongly saturated objective lens, the defocus induced by a variation of the lens current is up to a factor of two smaller than assumed in equation (1) due to the nonlinear response of the pole piece material.

The xy-noise contribution d_{noise} caused by deflectors, AC stray fields, and high-frequency stage vibrations cause *noise-induce image spread*, which increases the apparent size of the geometric image d_{src} of the virtual source at the specimen plane. Again we assume a Gaussian distribution for the individual contributions:

$$d_{\text{src}}^2 = d_{\text{geo}}^2 + d_{\text{noise}}^2 \qquad (2)$$

where d_{geo} denotes the size of the demagnified geometrical image of the virtual source.

To actually benefit from STEM resolution corresponding to the probe size, a sufficiently high axial brightness is required to obtain a high probe current. This leads to a good signal-to-noise ratio for the ADF detector signal and a sufficiently short dwell time to keep drift effects during image acquisition small.

The probe current I_{probe} is determined by the axial brightness β, the geometrical size of the virtual source d_{geo}, and the probe semiangle ϑ at the specimen plane:

$$\frac{I_{\text{probe}}}{\beta} = \frac{\pi^2}{4} d_{\text{geo}}^2 \vartheta^2. \qquad (3)$$

According to equation (3), the probe current is determined by d_{geo}, whereas for the probe size the xy-noise contribution to d_{src} must also be considered. This means the influence of xy-noise is different depending on the location where the noise is introduced. Noise caused by deflectors above the main demagnification stage of the condenser can be demagnified such that no increase of the probe size is observable. But in this case according to relation (3) also d_{geo} and, hence, the probe current is reduced. Noise introduced below the condenser, for example, by the scan coils, cannot be demagnified further and, therefore, always increases the STEM probe size. The latter directly affects the spatial resolution. Because ultimate STEM resolution is typically achieved at the brightness limit, the former mechanism also results in a loss of resolution due to the reduced signal-to-noise ratio at the ADF detector.

The probe size predicted from a theoretical model very much depends on the employed criterion. Care must be take when different results are compared. We consider the full-width-half-maximum diameter d_{fwhm} inappropriate to quantify STEM probe size, because this measure hardly accounts for the chromatic focus spread smearing out the current distribution at the probe position. Similarly, for a STEM with $C_3 > 0$, an increased aperture angle in combination with a strong defocus can be used to reduce d_{fwhm} considerably, but the proportion I_{fwhm} of the probe current I_{probe} actually contained within the disk of diameter d_{fwhm} drops down rapidly. Hence, if the d_{fwhm} criterion is used, the ratio $I_{\text{fwhm}}/I_{\text{probe}}$ should be calculated, also.

We prefer a probe size criterion more directly related to the distribution of the probe current. This is, for example, d_p (with $0 < p < 100$), where p percent of the total probe current is contained within the disk of diameter d_p. Common values for p are $p = 50$ or $p = 59$, because for a two-dimensional Gaussian distribution (brightness limited regime) one finds $d_{50} = d_{\text{fwhm}}$ and for the Airy function (diffraction limited regime) $d_{59} = 0.61(\lambda/\vartheta)$ corresponds to the Rayleigh criterion, where λ and ϑ denote the wavelength and the probe semiangle, respectively.

To predict the STEM probe profile, we extend the well-accepted procedure described, for example, by Kirkland (1998). The intensity profile of the probe situated at the center of the specimen plane is given by

$$I(w) = \frac{1}{\sqrt{2\pi\sigma_{\text{E}}^2}} \int \frac{1}{2\pi\sigma_{\text{src}}^2} \iint |\psi_{\text{probe}}(w - w', E')|^2 \times \exp\left(-\frac{1}{2} \frac{|w'|^2}{\sigma_{\text{src}}^2} \right) \times \exp\left(-\frac{1}{2} \frac{(E' - E_0)^2}{\sigma_{\text{E}}^2} \right) d^2w' \, dE', \qquad (4)$$

where w denotes the lateral coordinate. Equation (4) describes the convolution of the modulus of the wave function ψ_{probe} originating from a monochromatic point-shaped source with the energy spectrum and the lateral extension of the electron source. For both the energy distribution and the lateral extension, we assume Gaussian distributions with variance σ_{E} and σ_{src}, respectively. The angular emission of the source is almost constant within the range of the STEM aperture.

To calculate the wave function of the probe ψ_{probe}, we must account for the residual phase-shift $\gamma = \gamma(\alpha, E)$ introduced by the nonperfect optical system

$$\gamma(\alpha, E) = \frac{2\pi}{\lambda}\left(\chi(\alpha) + \frac{1}{2}\,\frac{E - E_0}{E_0}\,C_c|\alpha|^2\right). \tag{5}$$

The complex-valued aperture coordinate is $\alpha = \vartheta_x + i\vartheta_y$, with its complex-conjugate $\bar{\alpha}$, and $\chi = \chi(\alpha)$ denotes the point eikonal function. Off-axial aberrations and higher-order chromatic aberrations can be safely ignored for a STEM system. For a monochromatic, point-shaped virtual source, the probe function at the specimen plane is given by

$$\psi_{\text{probe}}(w) = \frac{1}{\sqrt{\pi}\lambda\vartheta}\iint_{|\alpha|<\vartheta}\exp\left(-i\,\frac{2\pi}{\lambda}\,\mathrm{Re}\{w\bar{\alpha}\}\right) \times \exp(-i\gamma(\alpha, E))\,d^2\alpha. \tag{6}$$

The multidimensional integral expression, which we obtain if we substitute equation (6) into (4), can be evaluated most efficiently by using the Fourier-convolution theorem and the fast Fourier transform (FFT).

The Eikonal function for Seidel orders $n \leq 7$ has the form

$$\begin{aligned}\chi(\alpha) = \mathrm{Re}\Big\{&\frac{1}{2}C_1\alpha\bar{\alpha} + \frac{1}{2}A_1\bar{\alpha}^2 + B_2\alpha^2\bar{\alpha} + \frac{1}{3}A_2\bar{\alpha}^3 \\ &+ \frac{1}{4}C_3\alpha^2\bar{\alpha}^2 + S_3\alpha^3\bar{\alpha} + \frac{1}{4}A_3\bar{\alpha}^4 \\ &+ B_4\alpha^3\bar{\alpha}^2 + D_4\alpha^4\bar{\alpha} + \frac{1}{5}A_4\bar{\alpha}^5 \\ &+ \frac{1}{6}C_5\alpha^3\bar{\alpha}^3 + S_5\alpha^4\bar{\alpha}^2 + R_5\alpha^5\bar{\alpha} + \frac{1}{6}A_5\bar{\alpha}^6 \\ &+ B_6\alpha^4\bar{\alpha}^3 + D_6\alpha^5\bar{\alpha}^2 + F_6\alpha^6\bar{\alpha} + \frac{1}{7}A_6\bar{\alpha}^7 \\ &+ \frac{1}{8}C_7\alpha^4\bar{\alpha}^4 + S_7\alpha^5\bar{\alpha}^3 + R_7\alpha^6\bar{\alpha}^2 \\ &+ G_7\alpha^7\bar{\alpha}^1 + \frac{1}{8}A_7\bar{\alpha}^8 + \ldots\Big\}.\end{aligned} \tag{7}$$

The traditional terminology for the eikonal coefficients with capital letters for the axial aberration figure and subscripts for the Seidel order as used in equation (7) is summarized in Table 1. For details about electron optical eikonal theory please consult, for example, Rose (2002).

Eikonal coefficients with multiplicity $\nu \neq 3k$, for $k = 0,1,2,\ldots$, do not arise in an ideal system consisting of hexapoles and round lenses only. For the ideal hexapole corrector, the second-order threefold astigmatism A_2 and the forth-order three-lobe aberration D_4 are also symmetry corrected. This means that in the fifth order only C_5 and A_5, in sixth order D_6, and in seventh order C_7 and G_7 can occur as residual intrinsic aberrations.

Residual Parasitic Aberrations

Optical aberrations limit the minimum attainable probe size. Therefore, it is required to derive upper limits for the acceptable residual parasitic aberrations. The larger the probe semiangle is and the smaller the target probe size becomes, the more stringent are these limits.

Whereas the minimization of the residual intrinsic aberrations is subject to the optical design of the corrector, the residual parasitic aberrations must be suppressed by an appropriate electro-mechanical construction of the corrector and must be minimized by appropriate alignment procedures during the operation of the system. For each relevant parasitic aberration, the corrector control software provides a so-called *alignment tool*. The alignment tool enables the user to correct for the corresponding aberration semiautomatically. The correction requires that the aberration has been measured before. The accuracy of this measurement process determines the amount of residual parasitic aberration still present after the alignment tool has been applied. If, as a result of an aberration measurement, all residual parasitic aberrations are zero within their confidence intervals, the state of the system is called *well aligned*.

The concept of alignment tools is based on the assumption that the alignment of the corrector is not too far away from the well-aligned state. Within this domain the alignment tools operate approximately linearly on the set of aberrations. If this assumption is not fulfilled, the alignment tools must be applied iteratively. For the present design of the hexapole corrector, alignment tools are available for all 12 components of the seven axial geometrical aberrations up to third order.

Upper limits for the residual aberrations of an aberration-corrected STEM have been calculated by Haider et al. (2000). The results given there refer to a target resolution of $d_{59} = 0.08$ nm at 200 kV. Today, about 6 years after this publication, under optimum conditions these limits can be met by the semiautomatic alignment procedures of the present CEOS STEM hexapole corrector CESCOR. Nevertheless, we are convinced that there is still considerable room for improvement with respect to to the accuracy of aberration measurement and the effectiveness of the alignment tools.

Results and Discussion

The Focus Spread Limit

The attainable minimum d_{50} probe size is limited by the focus spread of the probe-forming system. This is illustrated

Table 1. Terminology of the Eikonal Coefficients up to Seidel Order $n \leq 7$[a]

		Order n						
Name	Multiplicity	1	2	3	4	5	6	7
Defocus	$\nu = 0$	C_1						
nth order spherical aberration	$\nu = 0$			C_3		C_5		C_7
nth order axial coma	$\nu = 1$		B_2		B_4		B_6	
nth order star aberration	$\nu = 2$			S_3		S_5		S_7
nth order three-lobe aberration	$\nu = 3$				D_4		D_6	
nth order rosette aberration	$\nu = 4$					R_5		R_7
nth order pentacle aberration	$\nu = 5$						F_6	
nth order chaplet aberration	$\nu = 6$							G_7
νfold axial astigmatism	$\nu = n + 1$	A_1	A_2	A_3	A_4	A_5	A_6	A_7

[a]All four real-valued coefficients with multiplicity $\nu = 0$ and 19 complex-valued coefficients with multiplicity $\nu = 1, \ldots, 8$ are listed.

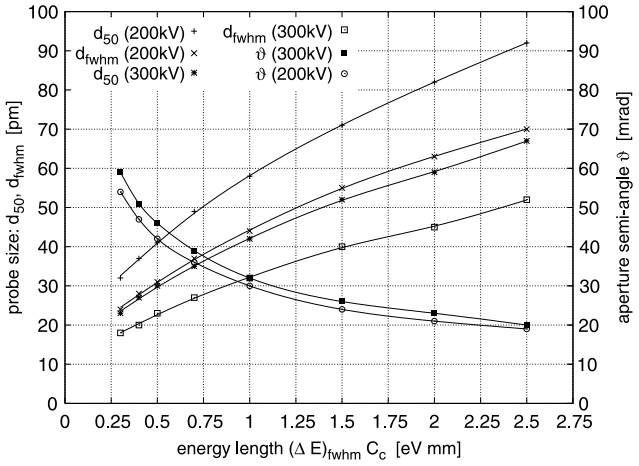

Figure 4. Minimum d_{50} and d_{fwhm} probe size and optimum aperture semiangle at the zero-current limit for an aberration-corrected STEM without any residual aberrations versus the energy length $(\Delta E)_{\mathrm{fwhm}} C_c$ for an acceleration voltage of 200 kV and 300 kV.

by Figure 4, where we plot different measures for the probe size and the optimum aperture angle for systems without any geometrical aberrations versus the energy length $(\Delta E)_{\mathrm{fwhm}} C_c$ for different acceleration voltages. The calculations have been performed according to equation (4) without taking any noise into account. The results refer to the zero-current limit; this means an infinitely demagnified image of the virtual source $d_{\mathrm{src}} \to 0$ is situated at the specimen plane. The probe semiangle ϑ has been chosen such that the resulting d_{50} probe size is minimum. For larger aperture angles, d_{50} would increase due to the chromatic focus spread, and for smaller aperture angles, it would increase due to diffraction.

For a given energy length, the optimum aperture semiangle is slightly smaller for 200 kV than for 300 kV, because the influence of the energy spread decreases with increasing acceleration voltage. On the other hand, the coefficient of the chromatic aberration and, hence, also the energy length is larger for a 300-kV objective lens than for a 200-kV lens with a comparable gap geometry. This is due to relativistic effects and due to the fact that saturation problems make the optimization of magnetic lenses less effective for higher beam energies. For an energy width of $(\Delta E)_{\mathrm{fwhm}} = 0.7$ eV the typical energy length including the contribution of the hexapole-corrector ranges from 1.0 mmeV for a 200-kV pole piece with a reduced gap size of about 3 mm to 1.7 mmeV for a 300-kV pole piece with a standard gap size of about 5 mm.

From Figure 4 we observe that the width d_{50} of the probe profile is always larger than d_{fwhm}. For probes limited by focus spread and diffraction, only about 36% of the total probe current is contained within the central disk of diameter d_{fwhm}, if the aperture angle is optimized for minimum d_{50}. A further increase of the semiaperture angle decreases d_{fwhm} further but $I_{\mathrm{fwhm}}/I_{\mathrm{probe}}$ drops down dramatically.

The results show that for 200 kV as well as for 300 kV the minimum probe size decreases considerably if the energy spread of the electron beam can be reduced with a gun monochromator (MC). For such an advanced MC-STEM, the optimum aperture angle is increased compared to a system without MC. This at least partially compensates for the anticipated brightness loss due to the filtering action of the MC.

The Residual Aberration Limit

For present-day STEM systems equipped with a hexapole corrector, the first nonvanishing residual intrinsic aberration is the fifth-order, sixfold astigmatism A_5. The fifth-order spherical aberration C_5 can be corrected by tuning the transfer lens system TL11/TL12 between the objective lens OL and the lower hexapole HP1. To achieve this C_5-free

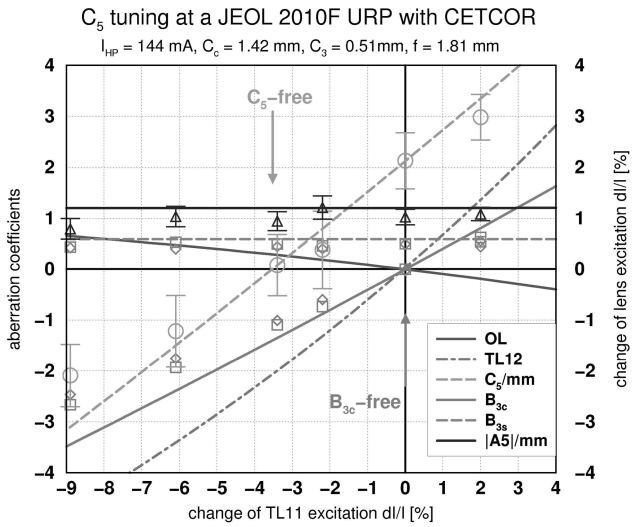

Figure 5. Experimental data compared with optical simulations. With a hexapole CTEM corrector, the excitation of the first transfer lens TL11 is tuned and the aberrations B_3, C_5, and A_5 are measured. The second transfer lens TL12 and the objective lens OL are used to compensate for defocus and residual C_3.

alignment, the central plane of HP1 is not imaged exactly at the coma-free aperture plane of the objective lens but at a distinct plane between the coma-free aperture plane and the specimen plane. In this case the additive primary contribution of the corrector and the objective lens to C_5 is exactly balanced against the secondary contribution owing to the combination effect between the negative $C_{3,\mathrm{HP}} < 0$ introduced by the corrector and the positive $C_{3,\mathrm{OL}} = -C_{3,\mathrm{HP}}$ of the objective lens. This advantageous effect has been pointed out by Rose (1971) and later applied to hexapole-type STEM correctors by Shao (1988). For C_5-free alignment the coma-free aperture plane of the corrector is not anymore optically conjugated with respect to the coma-free aperture plane of the objective lens; hence, the corrector contributes to the real-valued part B_{3c} of the off-axial coma $B_3 = B_{3c} + iB_{3s}$.

The experimental results of Hartel et al. (2004) depicted in Figure 5 approve the theoretical predictions. The experimental data and the simulation data depicted in Figure 5 refer to a hexapole CTEM corrector (JEOL 2010F URP with CETCOR). For the STEM hexapole corrector the situation is completely analogous, but, in contrast to CTEM, the increased off-axial coma B_3 does no harm in STEM because an appropriate scan strategy using the beam deflectors between the corrector and the objective lens can prevent this. Figure 5 shows how the relevant aberrations behave when the setting of the transfer lenses is tuned between B_{3c}-free alignment and C_5-free alignment. For $B_{3c} = 0$ the fifth-order spherical aberration amounts to $C_5 = 2.5$ mm, and for $C_5 = 0$, the real part of the off-axial coma is $B_{3c} = 2.0$ in dimensionless units. The excitation of the first transfer lens TL11 is reduced by 3.5% when going from B_{3c}-free to C_5-free alignment. The introduced defocus is compensated by changing the excitation of the objective lens and the second transfer lens TL12. Three parameters are required because, additionally, the condition of $C_3 = 0$ must be preserved. For a constant excitation of the hexapole elements HP1 and HP2, this implies that the magnification between the object plane and the intermediate image plane situated at the corrector's symmetry plane between transfer lenses TL21 and TL22 must be kept constant. The sixfold astigmatism $A_5 = 1.2$ mm, the imaginary part of the off-axial coma $B_{3s} = 0.65$ (unavoidable for a single-gap magnetic objective lens), and the total chromatic aberration $C_c = 1.42$ mm are not changed by this procedure. A good agreement between the measured aberrations and the simulation data is obvious.

The experiment described above should be considered as a proof of principle. Owing to the small $C_{3,\mathrm{OL}} = 0.50$ mm of the JEOL URP pole piece, C_5 is very small. Hence, for this small-gap objective lens pole piece, C_5-free alignment would hardly improve the STEM performance. Nevertheless, a MC-STEM equipped with a standard-gap objective lens pole piece can benefit from C_5-free alignment, especially because then no optimum balancing between C_5, C_3, and C_1 is required to obtain a minimum probe size.

Figure 6 compares the simulated current density profiles of the probes for a STEM system with and without hexapole corrector. In both simulations a realistic size of the source with respect to the specimen plane d_{src} but no residual parasitic aberrations have been taken into account. The calculation assumes a standard-gap objective lens pole piece with $C_{3,\mathrm{OL}} = 1.30$ mm and a chromatic aberration of $C_{c,\mathrm{OL}} = 2.0$ mm at a beam energy of 300 kV.

For the system without corrector, the probe size amounts to $d_{50} = 158$ pm or $d_{\mathrm{fwhm}} = 140$ pm for a probe aperture semiangle of $\vartheta = 8$ mrad and an optimum defocus of $C_1 = -38$ nm. The assumed size of the source is $d_{\mathrm{src}} = 60$ pm with respect to the specimen plane. For the system with hexapole corrector, we have, accordingly, $C_1 = C_3 = C_5 = 0$, $A_5 = 3.0$ mm, and $C_c = 2.4$ mm. With a probe semiangle of $\vartheta = 25$ mrad and a source size of $d_{\mathrm{src}} = 45$ pm, this results in a probe size of $d_{50} = 80$ pm or $d_{\mathrm{fwhm}} = 63$ pm. For the corrected system, the probe current is increased by a factor of five, whereas the probe size is reduced by a factor of two. Hence, as a benefit of C_s correction, the probe current is much more concentrated about the center of the probe. According to Figure 6, the corrected probe in underfocus and overfocus $C_1 = \pm 8$ nm has a sixfold shape. This is a direct consequence of the presence of the intrinsic residual sixfold astigmatism A_5 for the present design of the STEM hexapole corrector. The azimuthal orientation of the sixfold pattern rotates by 30° when switching from overfocus to underfocus. In Gaussian focus, the probe shape is rotationally symmetric as long as other residual aberrations can be neglected.

For the optimum resolution achievable with a present day high-resolution STEM equipped with a hexapole correc-

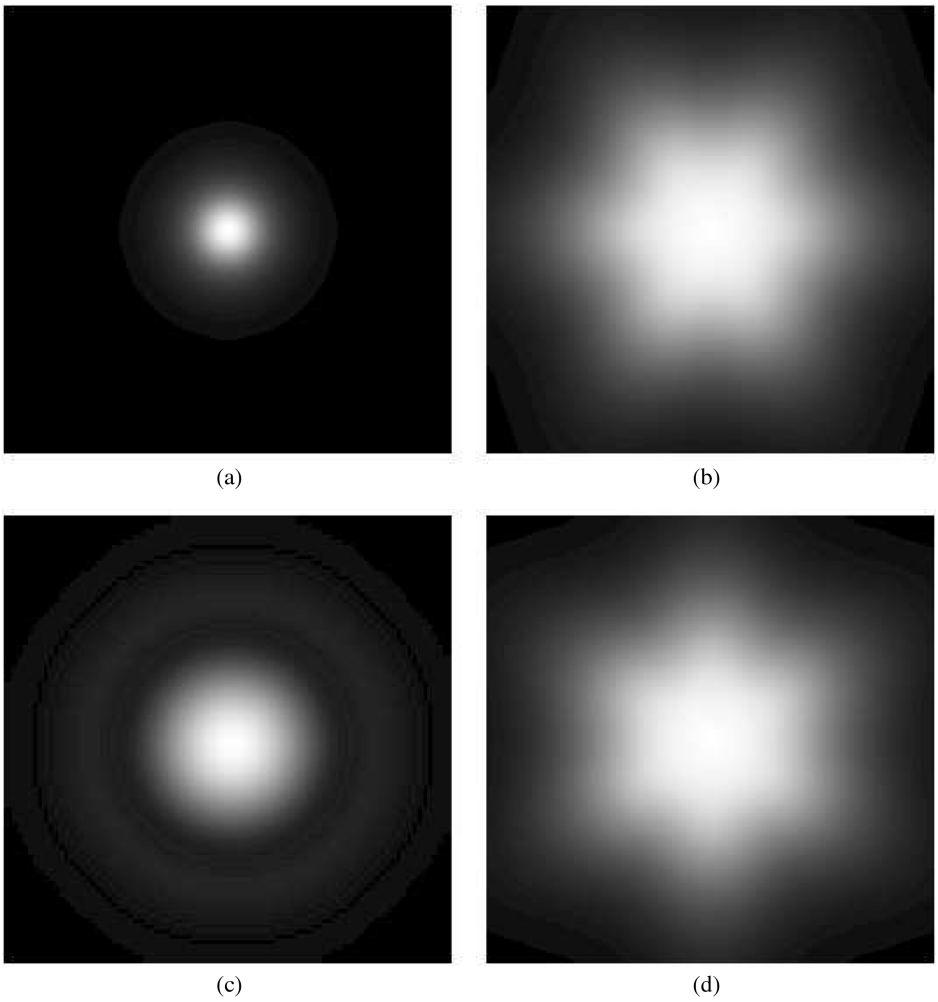

Figure 6. Simulated STEM probe profiles for a 300-kV system equipped with hexapole corrector in Gaussian focus $C_1 = 0$ nm (**a**), underfocus $C_1 = -8$ nm (**b**), and overfocus $C_1 = +8$ nm (**d**). For the calculation, we assume $C_c = 2.4$ mm, $\Delta E = 0.7$ eV (fwhm), $\theta = 25$ mrad, $A_5 = 3.0$ mm, $d_{\mathrm{src}} = 45$ pm, and no residual parasitic aberrations. For comparison, the probe profile for the uncorrected system with $C_3 = 1.30$ mm and optimum underfocus $C_1 = -38$ nm for $\theta = 8$ mrad and $d_{\mathrm{src}} = 60$ pm is shown (**c**). For all probes a square region of 0.63 nm is shown.

tor, residual intrinsic aberrations play a minor role. Figures 7 and 8 depict the probe size with respect to the zero-current limit as a function of the semiaperture angle for a 200-kV system with a reduced gap (3 mm) objective lens and a 300-kV system with a standard gap (5 mm) objective lens. In both cases we assume an energy width of $(\Delta E)_{\mathrm{fwhm}} = 0.7$ eV. For the 200-kV system a minimum probe size of $d_{50} = 58$ pm is obtained for $\vartheta = 30$ mrad. The aperture semiangle could be increased up to 35 mrad without strong effects of the aberrations on the probe size. This shows that for an objective lens with small C_c and small C_s STEM resolution of better than 70 pm is feasible even at 200 kV. For the 300-kV system, a slightly smaller minimum probe size of $d_{50} = 55$ pm is obtained for an optimum aperture semiangle of $\vartheta = 25$ mrad. Owing to the larger ratio $C_{3,\mathrm{OL}}/f_{\mathrm{OL}}$ for the standard gap lens, the A_5 introduced by the corrector is larger, and, hence, the probe size increases more strongly with a further increase of the aperture. Figures 7 and 8 again illustrate that d_{fwhm} is an improper measure for STEM probe size. The full-width-half-maximum of the probe profile decreases with increasing ϑ, but the

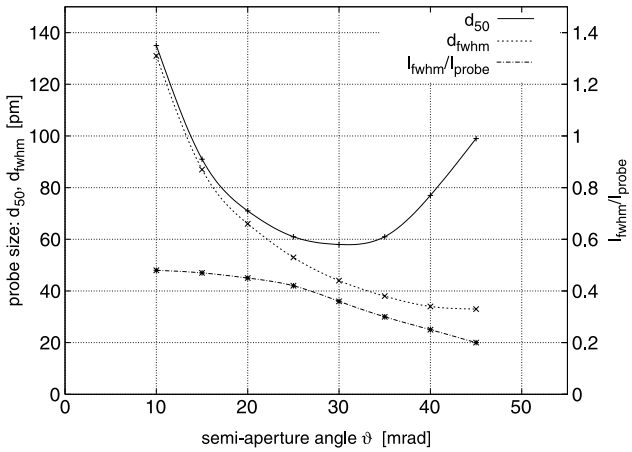

Figure 7. Simulated minimum probe size with respect to the zero-current limit $d_{\mathrm{src}} \to 0$ for a 200-kV STEM with hexapole corrector versus the aperture semiangle. The system is equipped with a reduced gap (3 mm) objective lens with $C_{3,\mathrm{OL}} = 0.5$ mm and $f_{\mathrm{OL}} = 1.8$ mm and has a total chromatic aberration of $C_c = 1.4$ mm, including the contributions of the hexapole corrector. An energy width of $(\Delta E)_{\mathrm{fwhm}} = 0.7$ eV has been assumed.

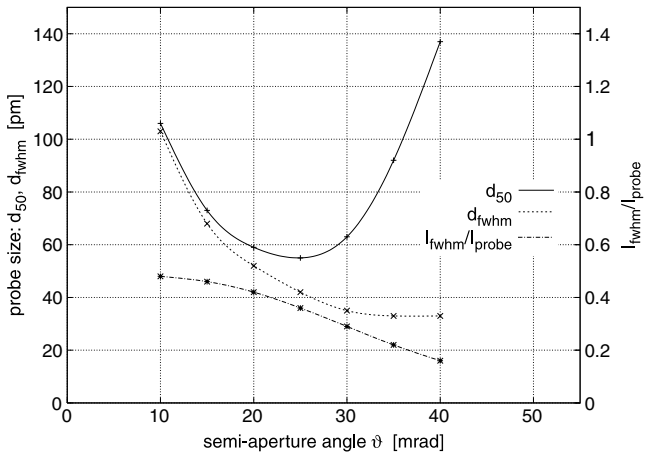

Figure 8. Simulated minimum probe size with respect to the zero-current limit $d_{src} \rightarrow 0$ for a 300-kV STEM with hexapole corrector versus the aperture semiangle. The system is equipped with a standard gap (5 mm) objective lens with $C_{3,OL} = 1.3$ mm and $f_{OL} = 2.3$ mm and has a total chromatic aberration of $C_c = 2.4$ mm, including the contributions of the hexapole corrector. An energy width of $(\Delta E)_{fwhm} = 0.7$ eV has been assumed.

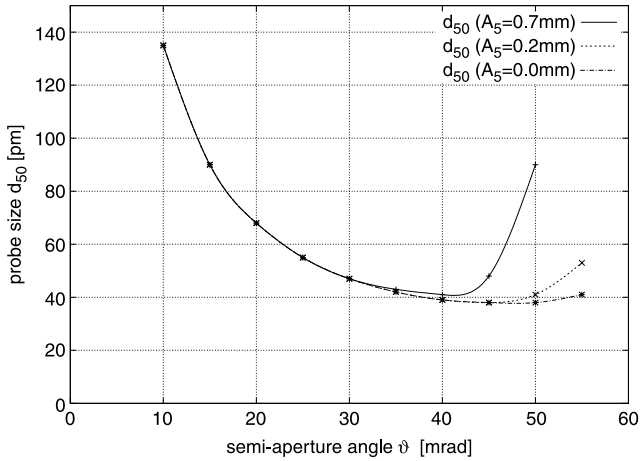

Figure 9. Simulated minimum probe size with respect to the zero-current limit $d_{src} \rightarrow 0$ for a 200-kV MC-STEM with hexapole corrector versus aperture semiangle and residual intrinsic A_5. The system is equipped with a reduced gap (3 mm) objective lens with $C_{3,OL} = 0.5$ mm and $f_{OL} = 1.8$ mm and has a total chromatic aberration of $C_c = 1.4$ mm, including the contributions of the hexapole corrector. A reduced energy width of $(\Delta E)_{fwhm} = 0.3$ eV has been assumed.

fraction of the probe current I_{fwhm}/I_{probe} actually contained in the disk of diameter d_{fwhm} drops down rapidly.

Summarizing the results depicted in Figures 7 and 8, we conclude that with the present design of the hexapole corrector in a STEM equipped with a standard FEG, the minimum STEM resolution is hardly affected by the residual sixfold astigmatism of the corrector. STEM resolution better than 70 pm should be feasible if all noise effects are sufficiently small and residual parasitic aberrations can be measured with good accuracy. This holds for 300-kV as well as for 200-kV systems, with the one limitation that for 200 kV an objective lens with small aberrations and, hence, reduced gap size should be used to obtain ultimate resolution. The requirements with respect to residual parasitic aberrations are slightly harder to meet at 200 kV owing to the larger aperture semiangle.

For an advanced STEM equipped with a MC-FEG the situation is different. Figures 9 and 10 show the influence of A_5 on the minimum probe size for a reduced energy width of $(\Delta E)_{fwhm} = 0.3$ eV. For the 300-kV system with standard gap OL, the effect is more pronounced than for the 200-kV system with reduced gap OL. To obtain a zero-current probe size below $d_{50} = 40$ pm, the probe semiangle should be increased at least by a factor of $\frac{3}{2}$ to counterbalance the loss of brightness owing to the MC. In this case the residual sixfold astigmatism should be as small as $|A_5| < 500$ μm for 300 kV and $|A_5| < 200$ μm for 200 kV. This demands for a considerable reduction of the aberration coefficient A_5 compared to the present design of the hexapole corrector.

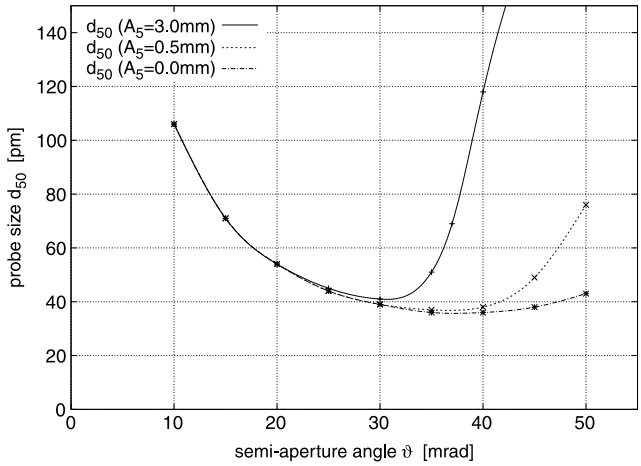

Figure 10. Simulated minimum probe size with respect to the zero-current limit $d_{src} \rightarrow 0$ for a 300-kV MC-STEM with hexapole corrector versus aperture semiangle and residual intrinsic A_5. The system is equipped with a standard gap (5 mm) objective lens with $C_{3,OL} = 1.3$ mm and $f_{OL} = 2.3$ mm and has a total chromatic aberration of $C_c = 2.4$ mm, including the contributions of the hexapole corrector. A reduced energy width of $(\Delta E)_{fwhm} = 0.3$ eV has been assumed.

Minimizing Fifth-Order Aberrations

A hexapole corrector optimized for a MC-STEM system should have minimized fifth-order residual aberrations. Hence, for an advanced MC-STEM, it is reasonable to

modify the design of the STEM hexapole corrector such that the fifth-order spherical aberration C_5 and the sixfold astigmatism A_5 can be reduced simultaneously. The strategy for C_5-free alignment with the STEM hexapole corrector has already been described. Additionally, if the condition $C_5 = 0$ is not met with sufficient precision, the residual C_5 can be balanced against C_3 and C_1 to reduce the impact of the residual phase shift on the STEM probe size.

Now, we turn to the residual sixfold astigmatism A_5. The modulus of the complex-valued aberration coefficient depends on the objective lens with focal length f_{OL} and spherical aberration $C_{3,\mathrm{OL}} > 0$ of the STEM system equipped with a hexapole corrector and the intermediate magnification M_{TL} between the objective lens and the corrector. Let us consider the axial fundamental ray u_α, starting with slope $u'_\alpha = 1$ at the specimen plane. Near the front-focal plane of the objective lens we find $u_\alpha = f_{\mathrm{OL}}$. Then, according to Figure 2, the height of the axial ray is constant inside the hexapole elements HP1 and HP2 with $|u_\alpha| = M_{\mathrm{TL}} f_{\mathrm{OL}}$. For a typical CESCOR system, the intermediate magnification is in the range of $0.5 \leq M_{\mathrm{TL}} \leq 1.0$. Approximately, the scaling rules

$$|A_5| \propto \left(\frac{C_{3,\mathrm{OL}}}{M_{\mathrm{TL}} f_{\mathrm{OL}}} \right)^2, \tag{8}$$

$$I_{\mathrm{HP}} \propto \sqrt{\frac{C_{3,\mathrm{OL}}}{M_{\mathrm{TL}}^4 f_{\mathrm{OL}}^4}} \tag{9}$$

hold, where I_{HP} denotes the current driving the hexapole elements. The range of validity of the first relation (8) is limited, as we will discuss later.

Equations (8) and (9) suggest we increase the intermediate magnification M_{TL} and decrease the excitation of the hexapole elements accordingly, in order to reduce the sixfold astigmatism. Unfortunately, the contribution of the corrector's transfer lenses to the total chromatic aberration of the probe-forming system increases quadratically with M_{TL}.

The simulation data depicted in Figure 11 illustrates this behavior. The hexapole currents have been tuned from $I_{\mathrm{HP}} = 70$ mA to $I_{\mathrm{HP}} = 140$ mA. The intermediate magnification is adjusted accordingly to keep $C_3 = 0$. The numerical results have been obtained for a standard gap objective lens at 300 kV. For a 200-kV system, the behavior would be very similar. For the system's nominal hexapole current of 135 mA, the total chromatic aberration amounts to $C_c = 2.4$ mm, which is about 20% more than for the object lens prefield alone, and the sixfold astigmatism is $|A_5| = 2.8$ mm. The simulation shows that the sixfold astigmatism can be reduced below $|A_5| < 1.0$ mm if the hexapole current is reduced to below 78 mA. This procedure simultaneously increases the total chromatic aberration to $C_c = 2.6$ mm. Because without MC the optical performance is limited by

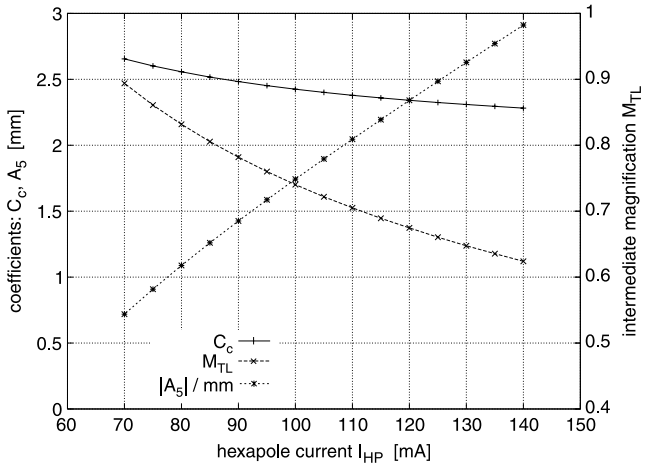

Figure 11. Residual aberrations C_c and A_5 for a STEM equipped with hexapole corrector depending on the excitation of the hexapole elements. The intermediate magnification M_{TL} and the specimen z-height z_{spec} must be adjusted accordingly. The calculation has been performed for a system with a standard gap objective lens at 300 kV.

the chromatic focus spread, the preferred mode of operation must be a rather strong hexapole current. Even for an MC-STEM, C_c is still an issue in keeping the required filter factor of the MC acceptable. However, in this case a certain trade-off between C_c and A_5 may be appropriate.

A second route to minimize A_5 is to reduce the length of the hexapole elements. To understand this, we briefly review the optical principle of a hexapole corrector. For this corrector design, the correction effect is based on combination aberrations of the threefold astigmatism A_2 of the hexapole fields with the hexapole fields themselves. The negative third-order spherical aberration $C_{3,\mathrm{HP}}$ introduced by the corrector is, hence, a secondary aberration. Therefore, both hexapole fields of the corrector must be sufficiently extended in the z-direction.

The theoretical analysis of the hexapole corrector reveals that in addition to the desired rotational symmetric $C_{3,\mathrm{HP}} < 0$, the hexapole elements introduce further axial aberrations. The three-lobe aberration showing up as a secondary aberration in the fourth order is corrected at the image plane. At least for the idealized corrector we find $D_4 = 0$, because the contributions of the first and the second hexapole to D_4 have opposite signs and chancel each other.

The contribution of the hexapole fields to the sixfold astigmatism in the fifth order can be classified as a ternary aberration. Ternary aberrations are combination aberrations induced by secondary aberrations. For A_5 the contributions of the first and second hexapole have the same orientation and, hence, add up. Fortunately, the magnitude of A_5 depends more strongly on the length of the hexapole elements than the corrector's $C_{3,\mathrm{HP}}$. Therefore, reducing the

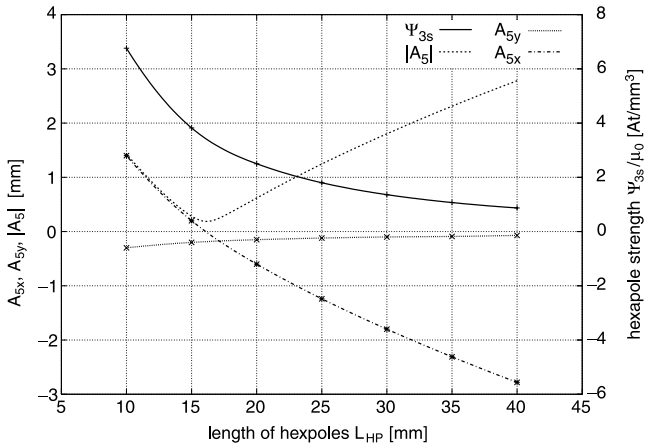

Figure 12. Sixfold astigmatism A_5 for a STEM equipped with hexapole corrector as a function of the length L_{HP} of the hexapole fields. The hexapole current I_{HP} must be adjusted accordingly to keep C_3 corrected. The calculation has been performed for a system with a standard gap objective lens at 300 kV.

length of the hexapole elements, while their excitation is increased to keep C_3 constant, reduces the residual A_5. We find the following approximate scaling rules:

$$I_{HP} \propto \frac{1}{L_{HP}^{3/2}}, \tag{10}$$

$$A_5 \propto L_{HP}, \tag{11}$$

where L_{HP} denotes the length of the hexapole fields and I_{HP} is the hexapole current required to keep C_3 corrected. To derive the second scaling rule (11) we consider only the contributions of the main hexapole fields. The influence of the transfer lenses and of the fringe fields is neglected. Due to this oversimplification, the relation (11) has a limited range of validity. For small values of L_{HP} it gives inaccurate results. This behavior will be discussed later.

In Figure 12, the residual A_5 and the required hexapole strength are plotted against the length of the hexapole elements. For $L_{HP} > 25$ mm the linear scaling rule (11) is approximately reproduced for $|A_5|$. Below the orientation of the sixfold astigmatism starts to change. The decrease of the modulus becomes superlinear. The exact calculations show that a nonzero minimum of $|A_5| = 190\ \mu$m is obtained for a hexapole length of $L_{HP} = 16$ mm. If A_5 is measured with respect to the coordinate system of the hexapole fields with odd orientation, the real component vanishes where $|A_5|$ is minimum. The calculations shown in Figure 12 have been performed for a standard gap OL at 300 kV. The results for a 200-kV STEM would be very similar.

To understand the behavior of A_5 with respect to I_{HP} and L_{HP} becoming apparent by the exact calculations we must recognize that not only the hexapoles but also the round lenses of the transfer doublet TL21/TL22 between the hexapoles contribute to the axial aberrations of multiplicity three and six. This contribution results from a combination of third-order aberrations of the transfer lenses and the threefold astigmatism introduced by the hexapole elements. Whereas contributions of TL21 and TL22 to the three-lobe aberration D_4 have opposite signs and, hence, cancel, contributions to A_5 add up for TL21 and TL22. This additional contribution causes the superlinear decrease of A_5 shown in Figure 12. It depends weakly on the gap geometry of the transfer lenses. As long as A_5 is dominated by the contribution caused by the hexapole fields alone, the scaling rules (11) and (8) apply. For decreasing length L_{HP} or increasing $M_{TL}f_{OL}$, this condition is not sufficiently well fulfilled anymore.

The superlinear decrease of $|A_5|$ and the minimum obtained for a positive length L_{HP} are considered an important finding. This effect enables the strong suppression of A_5 for a feasible electro-mechanical design, as it is required of the realization of an advanced hexapole corrector optimized for an MC-STEM.

For the sake of completeness we should mention that hexapole fringe fields can also contribute to $|A_5|$, but for the hexapole corrector these contributions are very weak and, therefore, negligible. In addition to the minimization of A_5 using the procedures described above, it is possible to directly correct for the sixfold astigmatism by one or more dodecapole fields. A possible solution would be to superimpose dodecapole fields to the hexapole fields. With this extra effort the residual A_5 could be nullified completely.

Performance of an MC-STEM

According to our results, the design of the hexapole corrector can be optimized with respect to the requirements of an advanced C_s-corrected MC-STEM.

For an objective lens with a standard gap size of about 5 mm operating at 300 kV, the residual sixfold astigmatism should be reduced below $|A_5| < 0.5$ mm to avoid limitations for an aperture semiangle of $\vartheta = 37.5$ mrad. The required reduction of A_5 is readily obtained by shrinking the length of the hexapole fields by a factor of two compared to the present design. In this case the hexapole strength must be increased by approximately a factor of three, which is considered feasible. With the monochromator we can obtain an energy width of $(\Delta E)_{fwhm} = 0.3$ eV with a filter factor of about $F_{MC} = 0.5$. The filter factor is defined as the ratio of the beam current with and without filtering. According to Figure 14, at 300 kV a probe size of $d_{50} = 37$ pm is possible with respect to the zero-current limit. To obtain a probe size of $d_{50} = 50$ pm we can allow for $d_{src} = 26$ pm. With a brightness of $\beta_{300kV} = 0.8 \times 10^9$ A/srcm^2, a MC filter factor of $F_{MC} = 0.5$, and a noise budget of $d_{noise} = 10$ pm, this corresponds to a probe current of $I_{probe} = 8$ pA.

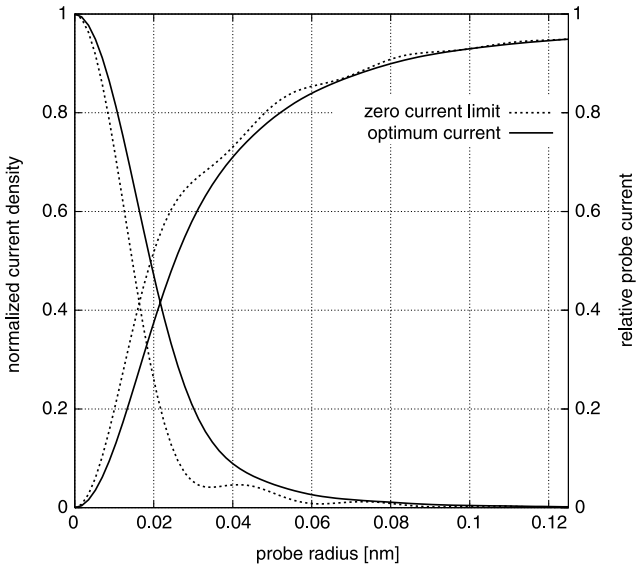

Figure 13. Calculated probe profile for a 200-kV MC-STEM with advanced hexapole corrector and reduced gap objective lens. For the simulation, the parameters $A_5 = 200\ \mu$m, $C_c = 1.4$ mm, $(\Delta E)_{\text{fwhm}} = 0.3$ eV, and $\vartheta = 45$ mrad have been assumed. The probe size with respect to the zero-current limit amounts to $d_{50} = 39$ pm. For $d_{50} = 50$ pm and maximum probe current, we can allow for an effective source size of $d_{\text{src}} = 24$ pm.

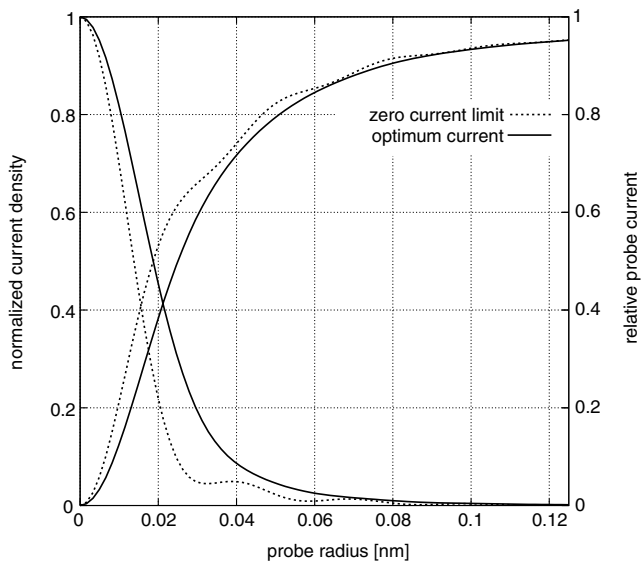

Figure 14. Calculated probe profile for a 300-kV MC-STEM with advanced hexapole corrector and standard gap objective lens. For the simulation, the parameters $A_5 = 500\ \mu$m, $C_c = 2.4$ mm, $(\Delta E)_{\text{fwhm}} = 0.3$ eV, and $\vartheta = 37.5$ mrad have been assumed. The probe size with respect to the zero-current limit amounts to $d_{50} = 37$ pm. For $d_{50} = 50$ pm and maximum probe current, we can allow for an effective source size of $d_{\text{src}} = 26$ pm.

For an objective lens with a reduced gap of about 3 mm operating at 200 kV, the residual sixfold astigmatism should be reduced below $|A_5| < 0.2$ mm to avoid limitations for an aperture semiangle of $\vartheta = 45$ mrad. The required reduction of A_5 is again obtained by shrinking the length of the hexapole fields by a factor of two compared to the present design. According to Figure 13 a probe size of $d_{50} = 39$ pm is possible with respect to the zero-current limit. To obtain a probe size of $d_{50} = 50$ pm, we can allow for $d_{\text{src}} = 24$ pm. With a brightness of $\beta_{200\,\text{kV}} = 0.5 \times 10^9$A/srcm^2, a MC filter factor of $F_{\text{MC}} = 0.5$, and a noise budget of $d_{\text{noise}} = 10$ pm, this corresponds to a probe current of $I_{\text{probe}} = 6$ pA.

Figures 13 and 14 depict the probe profiles with respect to the zero-current limit and for optimum probe current for an advanced C_s-corrected MC-STEM operating at 200 kV and 300 kV, respectively. The increased aperture for the 200-kV system nearly compensates for the lower brightness of the 200-kV system compared to the 300-kV system. The predicted probe currents are rather small but should be sufficient to demonstrate 50-pm STEM resolution.

The results show that even for a target probe size of $d_{50} = 50$ pm, the performance of the 200-kV system is comparable to that of a 300-kV system if for the dedicated 200-kV system an objective lens optimized for small C_c is used. This lens optimization can be performed more effectively at lower acceleration voltages because saturation effects for a dedicated 200-kV lens are not as pronounced as for a 300-kV lens. The chromatic aberration of a 300-kV objective lens with a 5-mm gap size is typically about 30%–40% larger than that for a 200-kV objective lens with comparable gap geometry. Even if the objective lens designed for 300 kV is operated at 200 kV, the resulting C_c is still typically 10%–15% larger compared to a lens design truly optimized for 200 kV. Nevertheless, STEM resolution can be improved slightly by using an objective lens with a reduced gap size also for 300-kV acceleration voltage.

The performance of an MC-STEM with an advanced hexapole corrector very much depends on the performance of the gun monochromator. The MC should be capable of reducing the energy width by roughly a factor of two. The reduction of the brightness should not be larger than the filter factor. This requirement makes a monochromator concept that has no spatial dispersion with respect to the object plane preferable for an advanced MC-STEM to obtain a maximum probe current (Uhlemann & Haider, 2002).

Limits for Residual Aberrations

With the strong reduction of the residual intrinsic fifth-order aberrations described above, the fundamental preconditions for an advanced hexapole STEM corrector are achieved. The next uncorrected higher-order residual intrinsic aberrations are in sixth order, the three-lobe aberration D_6, and in seventh order, the spherical aberration C_7 and the chaplet aberration G_7 of multiplicity $\nu = 6$. Calculations performed for the improved design show that these aberrations are rather small and tolerable.

More critical than the residual intrinsic aberrations are the residual parasitic aberrations. Due to the increased aperture semiangles proposed for an advanced corrector, the tolerable limits are more severe. According to our previous discussion, this makes necessary a more precise determination of parasitic aberrations. This requirement is one of the most demanding issues for the development of an advanced hexapole corrector for the MC-STEM, but it is not specific for hexapole-type correctors. It applies equally for any other corrector design aiming for 50-pm STEM resolution, for example, a quadrupole-octupole C_s-corrector or even a STEM C_c/C_s-corrector.

A full analysis of parasitic and residual parasitic aberrations and their limits is out of the scope of our present investigation. But as a rule of thumb, we can state that the residual aberrations should be so small that the maximum residual phase shift induced across the aperture is less than $\pi/4$.

Because for an advanced corrector optimized for an MC-STEM the probe semiangle is increased by a factor of $\frac{3}{2}$, the upper limit for the residual aberrations of order n are reduced by the factor $(\frac{2}{3})^{n+1}$ compared to the specifications of the present system. This is a direct consequence of equation (7). The lower limits for the tolerable residual aberrations directly translate into more challenging requirements for the precision of the aberration measurement.

Stability Requirements

The influence of incoherent effects on the performance of an advanced C_s-corrected STEM has already been discussed. Noise-induced focus spread as well as noise-induced image spread must be suppressed as far as possible. Because noise effects are typically uncorrelated, different contributions add up quadratically according to equations (1) and (2), respectively. To make sure that the performance of the instrument is not degraded by noise effects, the source size d_{src} must be dominated by the geometrical size d_{geo}, and the focus spread must be dominated by chromatic effects even for the MC-FEG. Because, compared to a present-day STEM with hexapole corrector, the assumed effective source size as well as the assumed energy width are smaller by a factor of two, the budgets for lens current and high-voltage stability are also stricter by a factor of two. The first requirement can be fulfilled by a careful design of the deflector elements with low-noise power supplies. The feasibility of the second requirement should be demonstrated in a CTEM equipped with hexapole-corrector and gun monochromator. The stronger requirements with respect to stability and drift must be fulfilled by the corrector as well as by the base instrument.

Conclusion

Our investigations show that the optical performance of the present design of the STEM hexapole corrector used at 200 kV or 300 kV with a standard FEG is not limited by residual intrinsic aberrations such as the fifth-order spherical aberration or the sixfold astigmatism. The minimum STEM probe size feasible for a 200-kV and a 300-kV system is comparable if for the 200-kV system an objective lens with a reduced gap size optimized for low chromatic aberration is used. The theoretical limit for the STEM resolution is below 70 pm for the present system. This shows that the full potential of the present design of the STEM hexapole corrector has not yet been demonstrated experimentally.

A future improvement of STEM resolution is feasible for a STEM with reduced focus spread, for example, for a MC-STEM with reduced energy width. For this application we propose a modified design of the hexapole STEM corrector with drastically reduced fifth-order sixfold astigmatism and no fifth-order spherical aberration. The latter has already been achieved for the present design. By using such a system, a STEM resolution of 50 pm seems feasible at 200 kV as well as 300 kV from an optical point of view. The most critical issues for the realization of such a system are to correct for all parasitic aberrations with sufficient accuracy and to provide a good overall stability of the instrument.

It is our opinion that, with respect to parasitic aberrations and alignment tools, more detailed investigations should be carried out during the first stage of the development of an advanced C_s-corrected MC-STEM. Our experience with this type of alignment problem gives us confidence that an improvement of STEM resolution can also be achieved with an advanced hexapole corrector in combination with a gun monochromator in practice.

Acknowledgments

We gratefully acknowledge the enthusiastic work of Rolf Erni (FEI Company) for recording the micrograph of Si⟨112⟩ shown in Figure 1. This recording would have been impossible without the excellent Si⟨112⟩ sample of Lena Fitting and David A. Muller (Cornell University).

References

Delby, N., Krivanek, O.L., Murfitt, M.F. & Nellist, P.D. (2005). Design and testing of a quadrupole/octupole C_3/C_5 aberration corrector. *Microsc Microanal* **11**(Suppl. 2), 2130–2131.

Erni, R., Freitag, B., Hartel, P., Müller, H., Tiemeijer, P., van der Stam, M., Stekelenburg, M., Hubert, D., Specht, P. & Garibay-Febles, V. (2006). Atomic scale analysis of planar defects in polycrystalline diamond. *Microsc Microanal* **12**, 492–497.

Haider, M., Uhlemann, S., Schwan, E., Rose, H., Kabius, B. & Urban, K. (1998). Electron microscopy image enhanced. *Nature* **392**, 768–769.

Haider, M., Uhlemann, S. & Zach, J. (2000). Upper limits for residual aberrations for a high-resolution aberration corrected STEM. *Ultramicroscopy* **81**, 163–175.

Hartel, P., Müller, H., Uhlemann, S. & Haider, M. (2004). Residual aberrations of hexapole-type C_s-correctors. In *Proceedings of the 13th European Microscopy Congress*, Van Dyck, D. & Oostveldt, P. (Eds.), vol. I, pp. 41–42. Antwerp: The Belgian Society for Microscopy.

Hutchison, J.L., Titchmarsh, J.M., Cockayne, D.J.H., Doole, R.C., Hetherington, C.J.D., Kirkland, A.I. & Sawada, H. (2005). A versatile double aberration-corrected, energy filtered HREM/STEM for materials science. *Ultramicroscopy* **103**, 7–15.

Kirkland, E.J. (1998). *Advanced Computing in Electron Microscopy.* New York: Plenum Press.

Krivanek, O.L., Dellby, N. & Lupini, A.R. (1999). Towards sub-Å electron beams. *Ultramicroscopy* **78**, 1–11.

Krivanek, O.L., Nellist, P.D., Dellby, N., Murfitt, M.F. & Szilagyi, Z. (2003). Towards sub-0.5Å electron beams. *Ultramicroscopy* **96**, 229–237.

Müller, H., Uhlemann, S., Hartel, P. & Haider, M. (2005). Optical design, simulation and alignment of present-day and future aberration correctors for the transmission electron microscope. In *Proceedings of the Microscopy Conference (6th Dreiländertagung)*, p. 6. Davos: Paul Scherrer Institut.

Nellist, P.D., Chisholm, M.F., Dellby, N., Krivanek, O.L., Murfitt, M.F., Szilagyi, Z.S., Lupini, A.R., Borisevich, A., Sides, W.H., Jr. & Pennycook, S.J. (2004). Direct sub-Ångstrom imaging of a crystal lattice. *Science* **305**, 1741.

Rose, H. (1971). Abbildungseigenschaften sphärisch korrigierter elektronenoptischer Achromate. *Optik* **33**, 1–24.

Rose, H. (2002). Advances in electron optics. In *High-Resolution Imaging and Spectrometry of Materials*, Ernst, F. & Rühle, M. (Eds.), pp. 189–270. Berlin: Springer-Verlag.

Rose, H. (2004). Outline of an ultracorrector compensating for all primary chromatic and geometrical aberrations of charged-particle lenses. *Nucl Instrum Methods A* **519**, 12–27.

Shao, Z. (1988). On the fifth-order aberration in a sextupole corrected probe-forming system. *Rev Sci Instrum* **59**, 2429–2437.

Uhlemann, S. & Haider, M. (2002). Experimental set-up of a fully electrostatic monochromator for a 200-kV TEM. In *Proceedings of the 15th International Congress on Electron Microscopy*, Engelbrecht, J., Sewell, T., Witcomb, M., Cross, R. & Richards, P. (Eds.), vol. I, pp. 327–328. Durban: Microscopy Society of Southern Africa.